APPENDIX B

Numerical Simulations of the Steady and Unsteady Aerodynamic Characteristics of a Circulation Control Wing Airfoil

APPENDIX B

Numerical Simulations of the Steady and Unsteady Aerodynamic Characteristics of a Circulation Control Wing Airfoil

Yi Liu, Lakshmi N. Sankar, Robert J. Englar, Krishan K. Ahuja
Georgia Institute of Technology, Atlanta, GA 30332-0150

ABSTRACT

The aerodynamic characteristics of a Circulation Control Wing (CCW) airfoil have been numerically investigated, and comparisons with experimental data have been made. The configuration chosen was a supercritical airfoil with a 30 degree dual-radius CCW flap. Steady and pulsed jet calculations were performed. It was found that the use of steady jets, even at very small mass flow rates, yielded a lift coefficient that is comparable or superior to conventional high-lift systems. The attached flow over the flap also gave rise to lower drag coefficients, and high L/D ratios. Pulsed jets with a 50% duty cycle were also studied. It was found that they were effective in generating lift at lower reduced mass flow rates compared to a steady jet, provided the pulse frequency was sufficiently high. This benefit was attributable to the fact that the momentum coefficient of the pulsed jet, during the portions of the cycle when the jet was on, was typically twice as much as that of a steady jet.

NOMENCLATURE

A_{jet}	= Area of Jet Slot
C	= Chord of Airfoil
C_L	= Lift Coefficients, L/qS
C_D	= Drag Coefficients, D/qS
C_μ	= Momentum Coefficient
$C_{\mu 0}$	= Average Momentum Coefficient for Pulsed Jet
D	= Drag of the Wing
f	= Pulsed Jet Frequency
L	= Lift of the Wing
$\dot{m}$	= Mass Flow Rate of Jet Blowing, slugs/sec
P	= Pressure
q	= Dynamic Pressure
S	= Area of the Wing
V_∞	= Free Stream Velocity
V_{jet}	= Jet Blowing Velocity
ρ_∞	= Free Stream Density
ρ_{jet}	= Jet Blowing Density

INTRODUCTION

In recent years, there has been an increasing demand for very large aircraft. At the same time, stringent restrictions on aircraft noise are being proposed by international aviation agencies. Noise pollution from the aircraft, especially around the airport, has becomes a major problem that needs to be solved. Airline operators, aircraft manufacturers, NASA, and FAA have all made noise reduction a priority.

These large aircraft will require sophisticated high-lift systems in order to use existing runways. A major source of airframe noise during take-off and landing is expected to be the high-lift system — namely the flaps, slats, and the flap-edges and gaps. These high-lift systems add to the weight of the aircraft, and are also costly to build and maintain.

An alternative to conventional high-lift systems is Circulation Control Wing technology. This technology and it aerodynamic benefits has been investigated over many years through experiment work[1,2] and numerical analyses[2,3,4]. A limited amount of work has also been done on the acoustic characteristics of Circulation Control Wings[5].

From these studies, it is known that very high C_L values (as high as 8.5 at α=0°) may be achieved with CCW airfoils. Because many mechanical components associated with high-lift systems are no longer needed, the wings can be lighter and less expensive to build. Major airframe noise sources, such as flap-edge noise, flap-gap noise, and flow-separation noise can all be eliminated with the use of CCW systems.

In view of the potential of CCW configurations, a coordinated research effort is underway at Georgia Tech involving wind tunnel tests, aeroacoustic tests, and CFD modeling. One of the goals of this research is to compare the aerodynamic and acoustic characteristics of a CCW configuration to that of a conventional high-lift system. A systematic study is also being done on the effects of slot size and placement on the wing lift, drag and noise characteristics. A third goal of this effort is to explore the use of pulsed jets for lift enhancement on CCW airfoils. A supercritical airfoil with a simple hinged dual-radius CCW flap shown in Figure 1 is used in much of this research. From existing experimental data[2], it is known that this CCW hinged flap design with lower flap angle of 30° can maintain most of the Circulation Control high lift advantages, while greatly reducing the drag that arises from

APPENDIX B

CCW airfoils with a rounded trailing edge and/or larger flap angles.

This paper is limited to the exploration of Circulation Control characteristics of the airfoil shown in figure 1. Two-dimensional study has been done, and preliminary comparisons with experimental data are presented. Preliminary unsteady simulations have also been done to understand the stall and vortex shedding characteristics of the wing/airfoil at high angles of attack and low levels of blowing. Companion studies for a 3-D finite wing may be found in Ref. 6.

MATHEMATICAL AND NUMERICAL FORMULATION

Computational Grid

A hyperbolic three-dimensional C-H grid generator is used in all the calculations. The three-dimensional grid is constructed from a series of two-dimensional C-grids with an H-type topology in the spanwise direction. The grid is clustered in the vicinity of the jet slot and the trailing edge to accurately capture the jet behavior over the airfoil surface.

Unsteady Navier-Stokes Solver

An Unsteady three-dimensional compressible Navier-Stokes solver is being used. The solver can model the flowfield over isolated wing-alone configurations. Both 3-D finite wings and 2-D airfoils may be simulated with the same solver.

The grid generation and the surface boundary condition routines are general enough so that one can easily vary the slot location, slot size, blowing velocity and direction of blowing. The effects of turbulence are modeled using either a Baldwin-Lomax eddy viscosity model, or a Spalart-Allmaras one–equation model. For a detailed discussion of the numerical solution procedure and the turbulence model, the reader is referred to Ref. 7.

Jet Boundary Conditions

In Circulation Control Wing studies, the driving parameter is the momentum coefficient, C_μ, defined as follows.

$$C_\mu = \frac{V_{jet} * \dot{m}}{S * \frac{1}{2}\rho_\infty V_\infty^2} \qquad (1)$$

Here, the jet mass flow rate is given by:

$$\dot{m} = \rho_{jet} V_{jet} * A_{jet} \qquad (2)$$

In the present study, the jet is subsonic, and the following boundary conditions are specified at the slot exit: the total temperature of the jet, the momentum coefficient C_μ as a function of time, and the flow angle at the exit. In this simulation, the jet was tangential to the airfoil surface at the exit. All other parameters were computed using ideal gas law, and through an extrapolation of the Riemann variables (carried by upstream traveling acoustic waves) that enter the subsonic jet slot from the exterior. It may be noted that in the experiment, the flow conditions were such that the exit static pressure at the slot equals the ambient static pressure.

RESULTS AND DISCUSSION

The initial studies were for a 2-D configuration to understand the high-lift, stall, and vortex shedding characteristics of the airfoil with and without blowing. Some comparisons have been made between the CFD results and the measured data. In parallel with this study, a finite aspect ratio wing was also analyzed to determine its C_{Lmax} with and without Circulation Control. Figure 1 shows the configuration studied. The CCW flap setting may be varied both in the experiments and the simulations. The studies presented here are all for the 30 degree flap setting.

In these studies, the free stream velocity was approximately 94.3 ft/sec at a dynamic pressure of 10 psf and an ambient pressure of 14.2 psia. The free stream density is about 0.00225 slugs/ft^3. These conditions translate into a free stream Mach number 0.0836 and a Reynolds Number of $3.95*10^5$, and were chosen to match the experiments done by Englar et al (Ref. 2).

Steady Jet Results:

Figure 2a shows the computed C_l vs. α curve, for a number of $C\mu$ values. The calculations correctly reproduce the decrease in the stall angle observed in the experiments at high momentum coefficients, attributable to leading edge stall (Englar, unpublished results). Figure 2b shows the variation of C_L with respect to $C\mu$ at a fixed angle of attack (α=0 degrees). Excellent agreement with measured data from Reference 2 is evident.

These simulations also give some insight into the physics of the flow. For example, consider a typical case at $\alpha = 0°$. Without any blowing, trailing edge separation and vortex shedding occurred and the lift coefficient varied from 0.768 to 0.854. The measured data had an average of 0.878. When Circulation Control was applied with a C_μ of 0.1657, the 2-D lift coefficient increased to a value of 3.07. This is in excellent (less than 1%) agreement with the measured value of 3.097. As will be discussed below, these values can be attained in conventional wings only with the use of complex flaps, which would considerably increase the mechanical complexity and weight of the wing. For comparison, a 30° Fowler flap on this same airfoil experimentally yielded C_L =1.8 at $\alpha = 0°$.

Figure 3 shows the lift coefficient variation with time. It is seen that the variation is periodic with a dimensional frequency around 400Hz for the flow conditions stated earlier. Figure 4 shows the streamlines around the airfoil for the blown and unblown cases. At a

typical instance in time, it is clearly seen that the trailing-edge vortex shedding, a potential source of noise, has been eliminated by Circulation Control.

Pulsed Jet Studies

During the past five years, there has been increased interest in the use of pulsed jets, and "massless" synthetic jets for flow control and performance enhancement. Wygnansky et al.[8, 9], Lorber et al.[10], and Wake et al[11] have studied the use of directed synthetic jets for static separation and dynamic stall alleviation. Hassan[12] has studied the use of synthetic jets placed on the upper and lower surfaces of an airfoil surface as a way of achieving desired changes in lift and drag, offsetting vibratory airloads that otherwise would occur during blade-vortex interactions. Pulsed jets and synthetic jets have also been used to effect mixing enhancement, thrust vectoring, and bluff body flow separation control. Pulsed blowing of blown flap configurations has also been investigated experimentally (Ref. 13). A combined CFD, experimental aerodynamics, and aeroacoustics study has been initiated at Georgia tech to understand and explore this very promising technology.

The present computational studies were aimed at answering the following questions: Can pulsed jets be used to achieve desired increases in the lift coefficient at lower mass flow rates relative to a steady jet? What are the effects of the pulsed jet frequency on the lift enhancement, for a given time-averaged C_μ? What is the optimum wave shape for the pulsed jet, i.e. how should it vary with time?

In the calculations below, the mean flow angle was set at zero, and the dual-radius CCW flap angle was fixed at 30 degree. The free stream Mach number, slot height, chordwise location of the slot, and angle of attack were all, likewise, held fixed. The pulsed jet characteristics are defined by the instantaneous momentum coefficient C_μ, which varies with time as follows:

$$C_\mu(t) = C_{\mu,0} + C_{\mu,0} F(f,t) \qquad (3)$$

A set of preliminary calculations were done using a sinusoidal function form - F(t) equal to $\cos(2\pi ft)$. It was found that this was not an effective wave shape to use. The computed C_l values simply oscillated about the mean value, so that the time averaged C_l values were no higher than the steady state values achieved with a fixed jet operating at the mean $C_{\mu 0}$ value. However, improved results were obtained when the function F(t) was chosen to be a square shape wave form with a 50% duty cycle. Under this setting, F(t)=1 for half the cycle, and F(t)=-1 for the other half of a cycle, as shown in Figure 5. The frequency "f" indicates the number of times the jet was turned on and off per second. Note that the instantaneous coefficient is thus zero during one half of the cycle, and equals 2 $C_{\mu 0}$ during the other half of the cycle, so that the time-averaged value is $C_{\mu 0}$.

Figure 6a and 6b show the variation of the time-averaged incremental lift coefficient ΔC_l over and above the base-line unblown configuration, at three frequencies, 40 Hz, 120 Hz and 400 Hz. These three frequencies correspond to Strouhal numbers f^*C/V_∞ equal to 0.2828, 0.8484 and 2.828 respectively. Figures 7a and 7b show the corresponding behavior of the time-averaged lift-to-drag ratio $C_l/(C_d+C_{\mu 0})$. Here, the drag coefficient has been corrected for the u-momentum imparted by the jet into the wake. For comparison, corresponding variations with a steady jet are also shown.

For a given value of C_μ, a steady jet gives a higher value of ΔC_l compared to a pulsed jet. This is to be expected because the pulsed jet is operational only half the time during each cycle where as the steady jet is continuously on. The benefits of the pulsed jet are more evident in figures 6b. At a given mass flow rate, it is seen that the time-averaged values of lift are higher for the pulsed jet case compared to the steady jet case, especially at higher frequencies. This superior performance of the pulsed jet can be explained as follows. The momentum coefficient is proportional to the square of the jet velocity, where as the mass flow rate is proportional to jet velocity V_{jet}. As a consequence, doubling the instantaneous momentum coefficient C_μ to twice its average value increases the instantaneous mass flow rate only by 40% (1.414 to be exact) compared to a steady jet. The Coanda effect, on the other hand, is dependent on the jet velocity squared, and greatly benefits from these brief increases in the momentum coefficient. This leads to higher lift, compared to a steady jet as seen on figure 6b. The L/D ratio for the steady jet is, however, still better compared to the pulsed jet case as seen on figures 7b, partly because the C_μ values of the steady jet case with same mass flow rate are lower than the pulsed jet case.

Pulsed jet calculations have also been done at a fixed time averaged value of $C_{\mu o}$ equal to 0.04, while parametrically changing the pulse jet frequency, f. Figure 8 shows these results. It is seen that higher frequencies are, in general, preferred over lower frequencies. Our simulations indicate that the airfoil needs to travel 4 to 6 chord lengths after the jet has been turned off before all the beneficial circulation attributable to the Coanda effect is completely lost. If a new pulse cycle could begin before this occurs, the circulation will almost instantaneously reestablish itself. At high enough pulse frequencies, as a consequence, the pulse jet will have all the benefits of the steady jet at considerably lower mass flow rates.

It should be noted here that Cμ was varied with time in a square wave at CFD simulation. In practice, it is more convenient to vary the plenum pressure, which controls Cμ, jet velocity and mass flow. If plenum pressure were varied in a square wave form (for pressure values from 0 to two times the average) it is expected that Figure 6a would also show increased ΔC_l over the steady state value, as shown in Ref. 13.

APPENDIX B

CONCLUDING REMARKS

Unsteady Reynolds-averaged Navier-Stokes calculations have been carried out for a supercritical airfoil equipped with a 30-degree dual-radius CCW flap. The predicted values of lift coefficient, when the airfoil is operating using Circulation Control are in excellent agreement with measurements. Calculations have also been done for a pulse jet configuration. It was found that the pulse jet configuration gave larger increments in lift compared to the steady jet, at a given time-averaged mass flow rate. This was attributed the fact that the pulsed jet had larger instantaneous momentum coefficients leading to enhanced Coanda effect. Finally, pulsed jet performance improved at higher pulse frequencies due to the fact that the airfoil had not shed the circulation into the wake before a new pulse cycle began.

While these simulations are very encouraging, additional calculations are needed to further define the optimum placement of slots, and to establish the minimum mass flow rates needed to achieve lift coefficients comparable to conventional high-lift systems. The noise penalty associated with a pulsed jet system must be assessed, and compared to the noise characteristics of conventional high-lift systems. These studies are now in progress.

REFERENCES

1. Englar, R.J. and Huson, G.G. "Development of Advanced Circulation Control Wing High Lift Airfoils", AIAA Paper 83-1847, presented at AIAA Applied Aerodynamics Conference, July, 1983.
2. Englar, Robert J., Smith, Marilyn J., Kelley, Sean M. and Rover, Richard C. III., "Development of Circulation Control Technology for Application to Advanced subsonic Transport Aircraft", AIAA Paper 93-0644, presented at AIAA Aerospace Sciences Meeting, January, 1993.
3. Shrewsbury, George D., "Analysis of Circulation Control Airfoils using an Implicit Navier-Stokes Solver", AIAA Paper 85-0171, January, 1985.
4. Shrewsbury, G. D., "Dynamic Stall of Circulation Control Airfoils", Ph.D Thesis, Georgia Institute of Technology, November 1990.
5. Salikuddin, M., Brown, W. H. and Ahuja, K. K., "Noise From a Circulation Control Wing with Upper Surface Blowing", Journal of Aircraft, Vol.24, Jan 1987, p55-64.
6. Yi Liu, "Numerical Solution of the Aerodynamic and Aeroacoustic Characteristics of Circulation Control Wings", Ph.D Proposal in preparation.
7. Wake, B.E., "Solution Procedure for the Navier-Stokes Equations Applied to Rotors", Ph.D. Thesis, Georgia Institute of Technology, Atlanta, GA 1987.
8. Seifert, A., Darabi, A. and Wygnanski, I., "Delay of Airfoil Stall by Periodic Excitation", AIAA Journal of Aircraft, Vol. 33, No. 4, 1996.
9. Wygnanski, I, "Some New Observations Affecting the Control of Separation by Periodic Excitation", AIAA 2000-2314, FLUIDS 2000 Conference and Exhibit, Denver, CO, 19-22 June, 2000.
10. Lorber, P.F., McCormick, D., Anderson, T., Wake, B.E., MacMartin, D., Pollack, M., Corke, T., and Breuer, K., "Rotorcraft Retreating Blade-Stall Control," AIAA 2000-2475, FLUIDS 2000 Conference and Exhibit, Denver, CO, 19-22 June, 2000.
11. Brian Wake and Elizabeth A. Lurie, "Computational Evaluation of Directed Synthetic Jets for Dynamic Stall Control," to appear in the American Helicopter Society Annual Forum, 2001.
12. Hassan, A., and Janakiram, R. D., "Effects of Zero-Mass Synthetic Jets on the Aerodynamics of the NACA 0012 Airfoil", Journal of the American helicopter Society, Vol. 43, No. 4, October, 1998.
13. Oyler, T.E. and W.E. Palmer, "Exploratory Investigation of Pulse Blowing for Boundary Layer Control," North American Rockwell Report NR72H-12, January 1972.

APPENDIX B

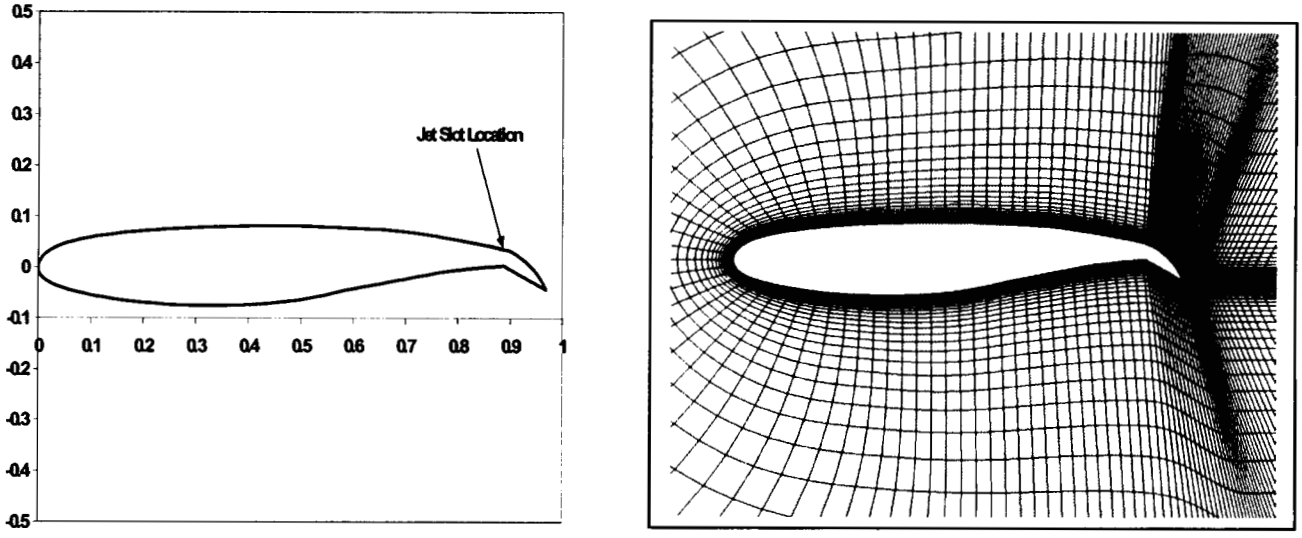

Figure 1. Circulation Control Wing Airfoil (with 30° dual-radius CCW flap) and the Body-Fitted Grid

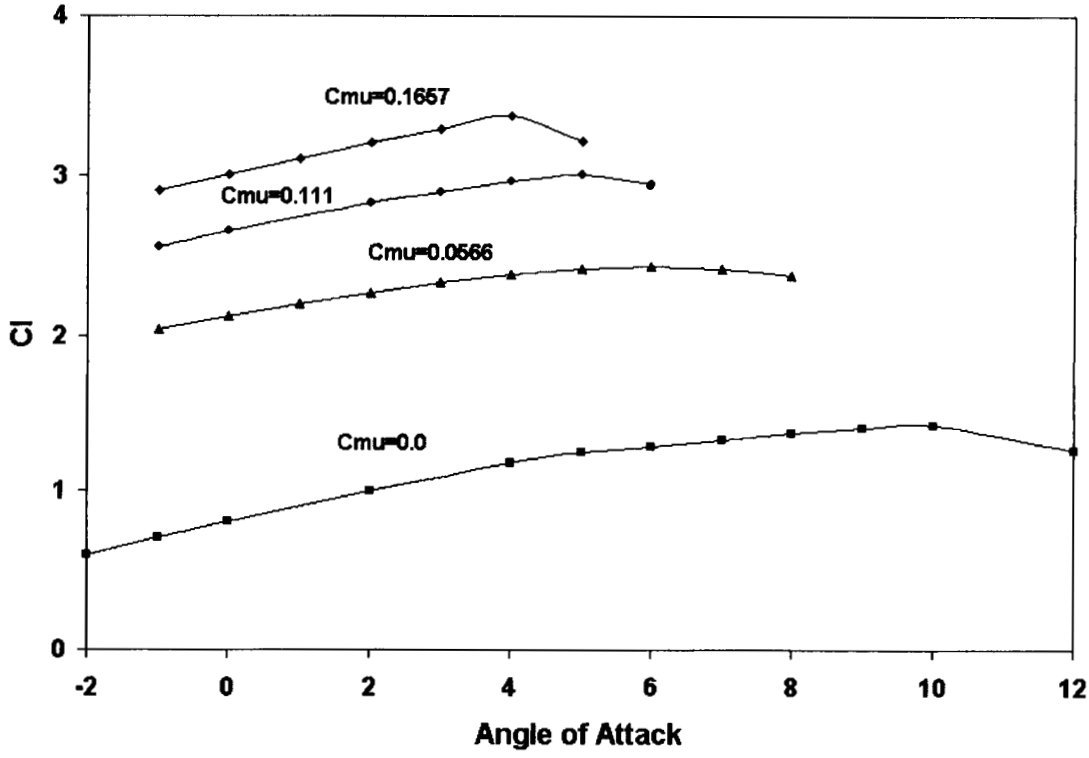

Figure 2a. The CFD-Computed Variation of Lift Coefficient with the Angle of Attack for the 30-degree CCW Flap Case

APPENDIX B

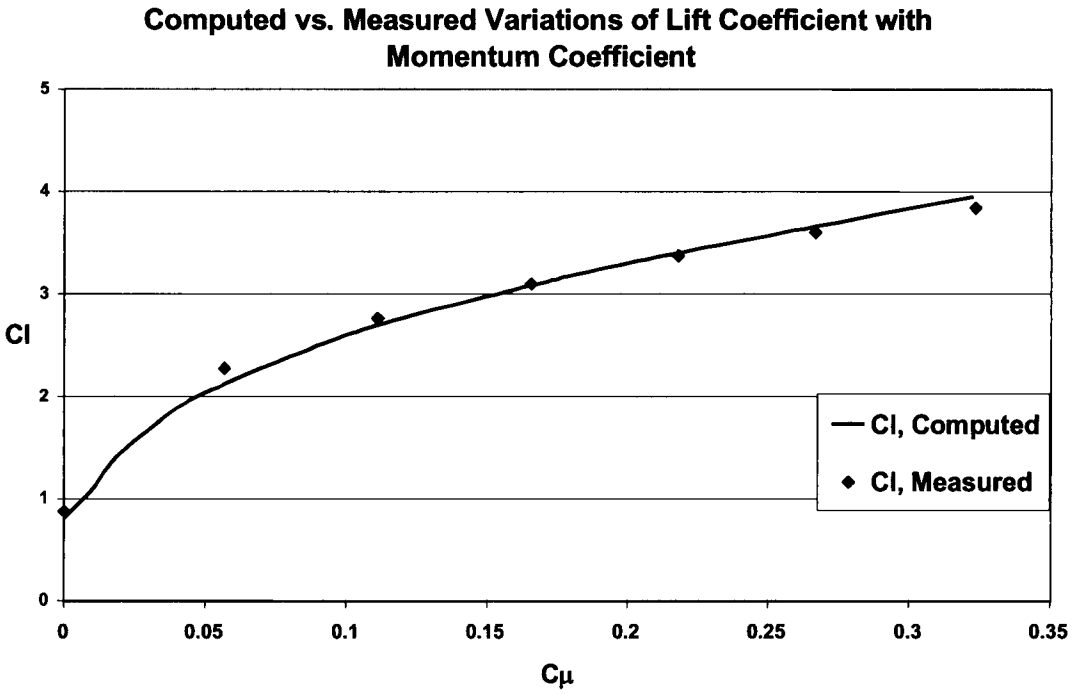

Figure 2b. Variation of the Lift Coefficient with Momentum Coefficient at α=0° and 30° Flap angle (For comparison, a comparable Fowler Flap system with 30-degree flap setting will have a C_l of 1.8)

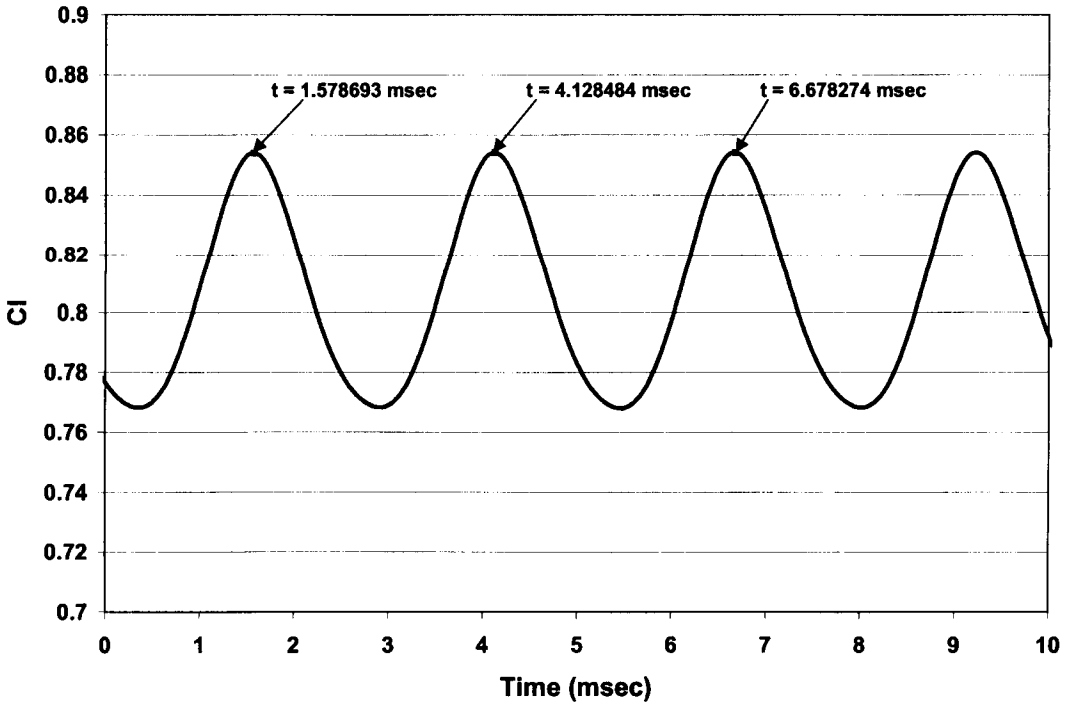

Figure 3. Lift Coefficient Variation with Time for the Unblown Case with a 30-degree Flap Setting (The Shedding Frequency is about 400 Hz)

APPENDIX B

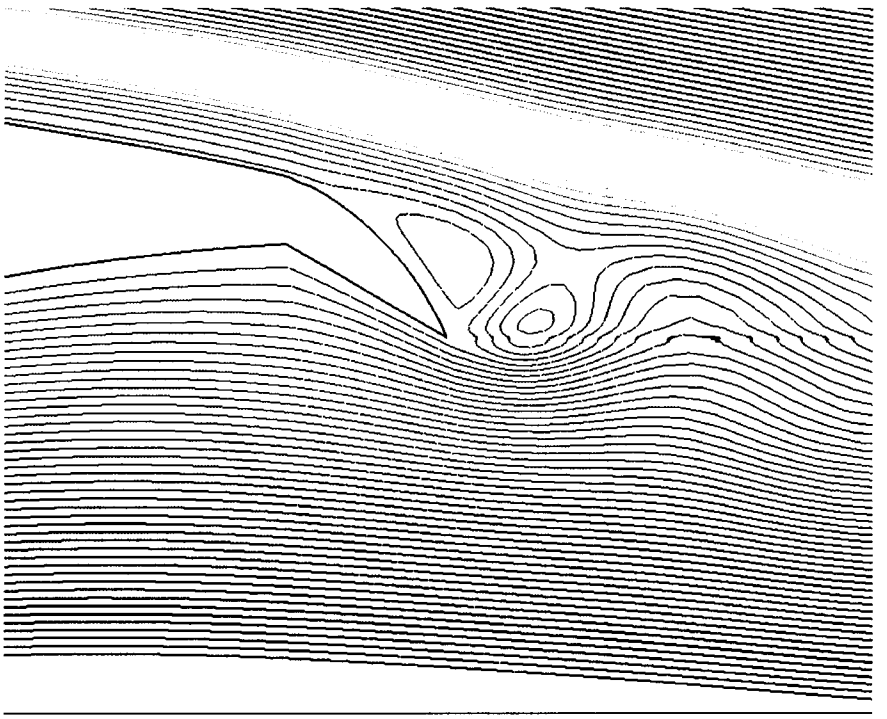

Figure 4a. The Stream Function Contour for the Unblown Case at 30 Degree Flap Setting

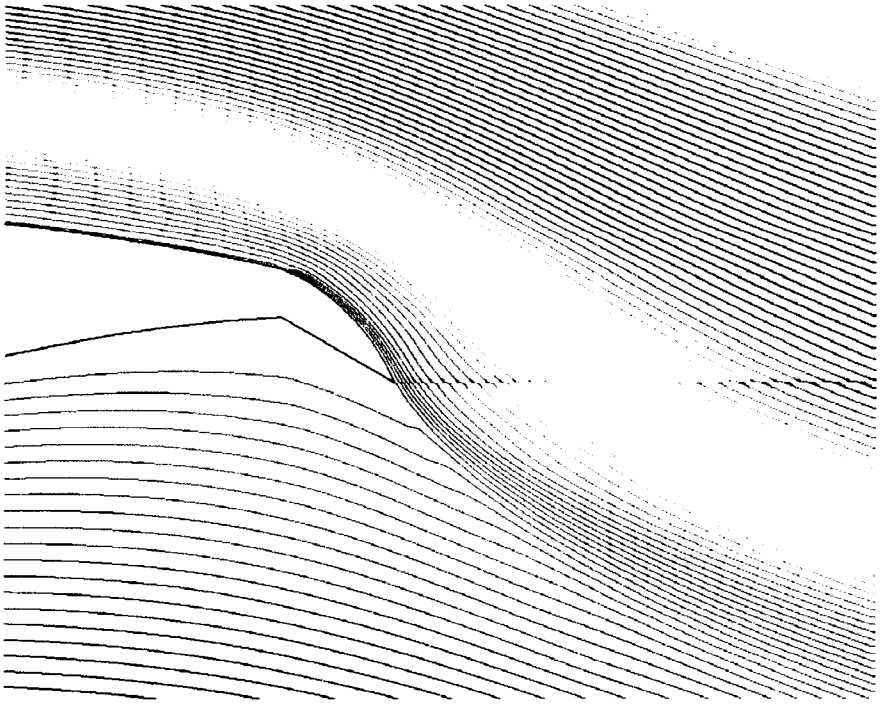

Figure 4b. The Stream Function Contour for the Blowing Case at 30 Degree Flap Setting, C_{μ}=0.1657

APPENDIX B

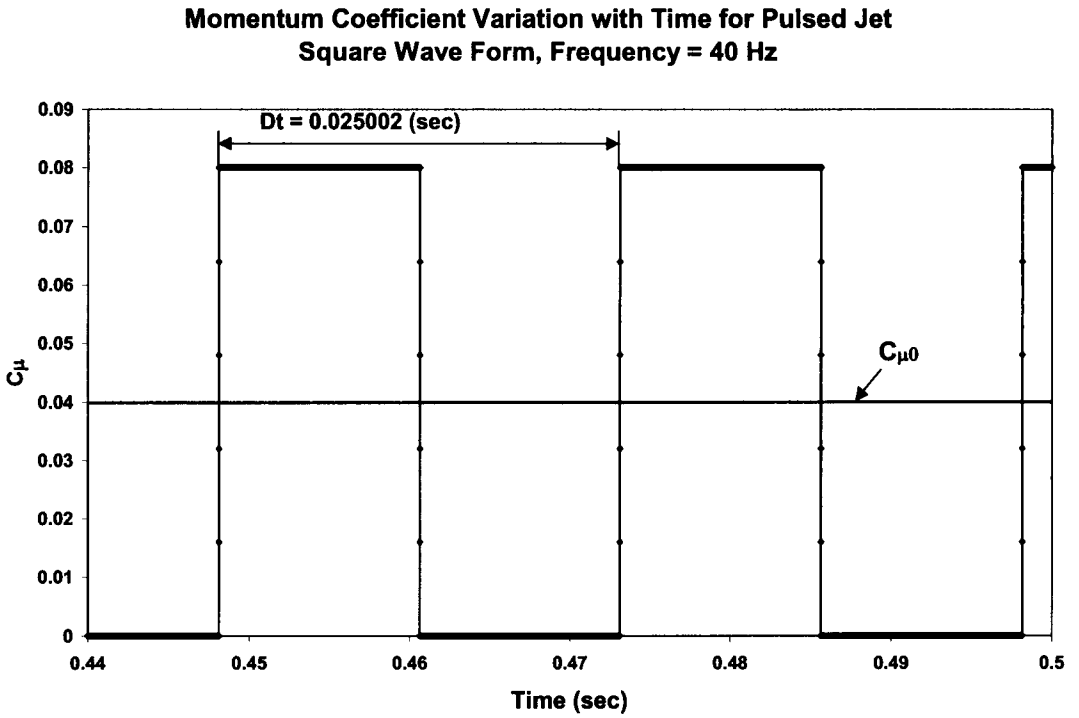

Figure 5. Variation of Momentum Coefficient with Time, Square Wave Form

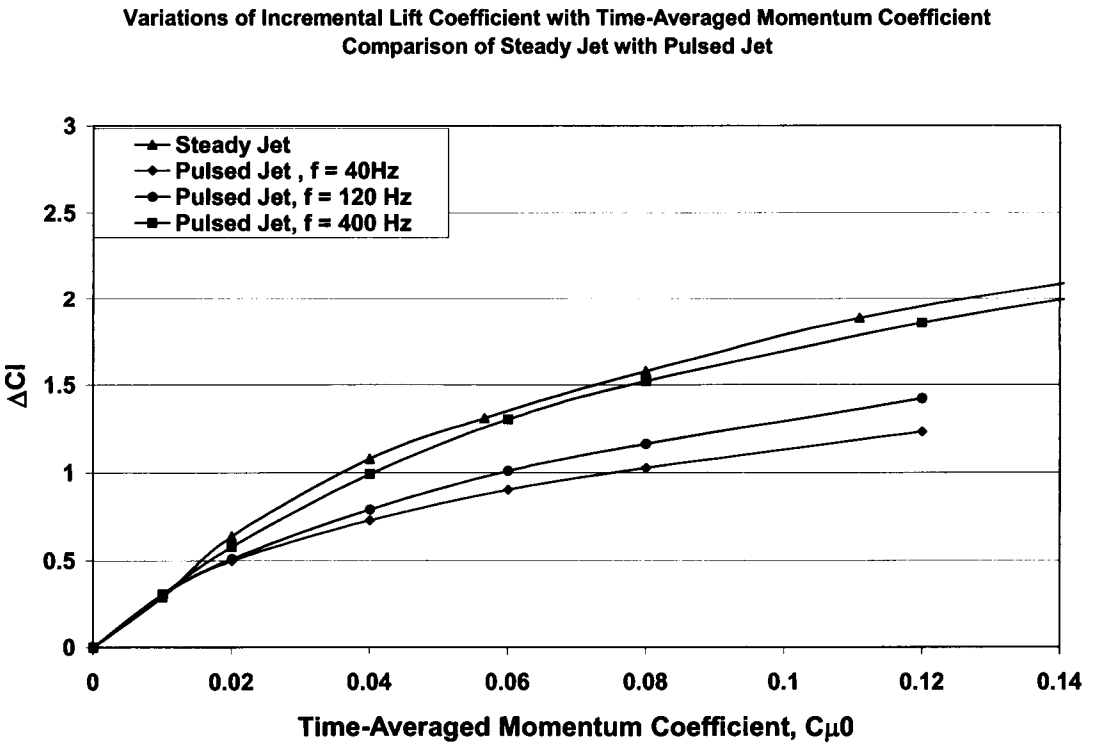

Figure 6a. Variation of Incremental Lift Coefficient with Time-Averaged Momentum Coefficient

APPENDIX B

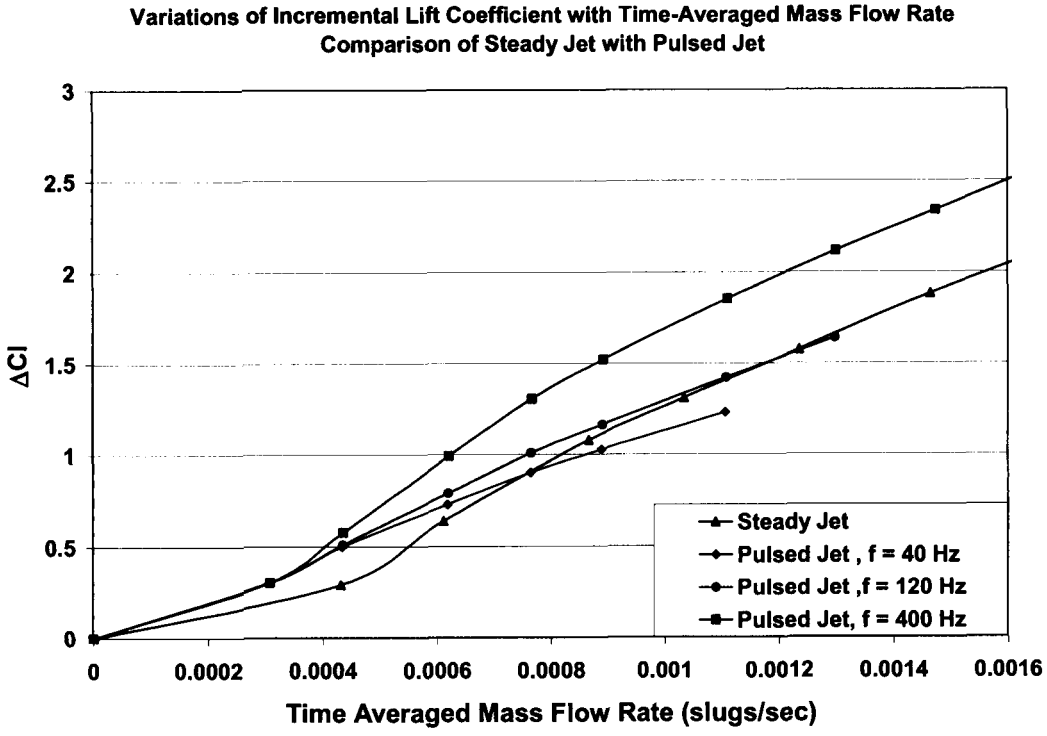

Figure 6b. Variation of Incremental Lift Coefficient with Time-Averaged Mass Flow Rate

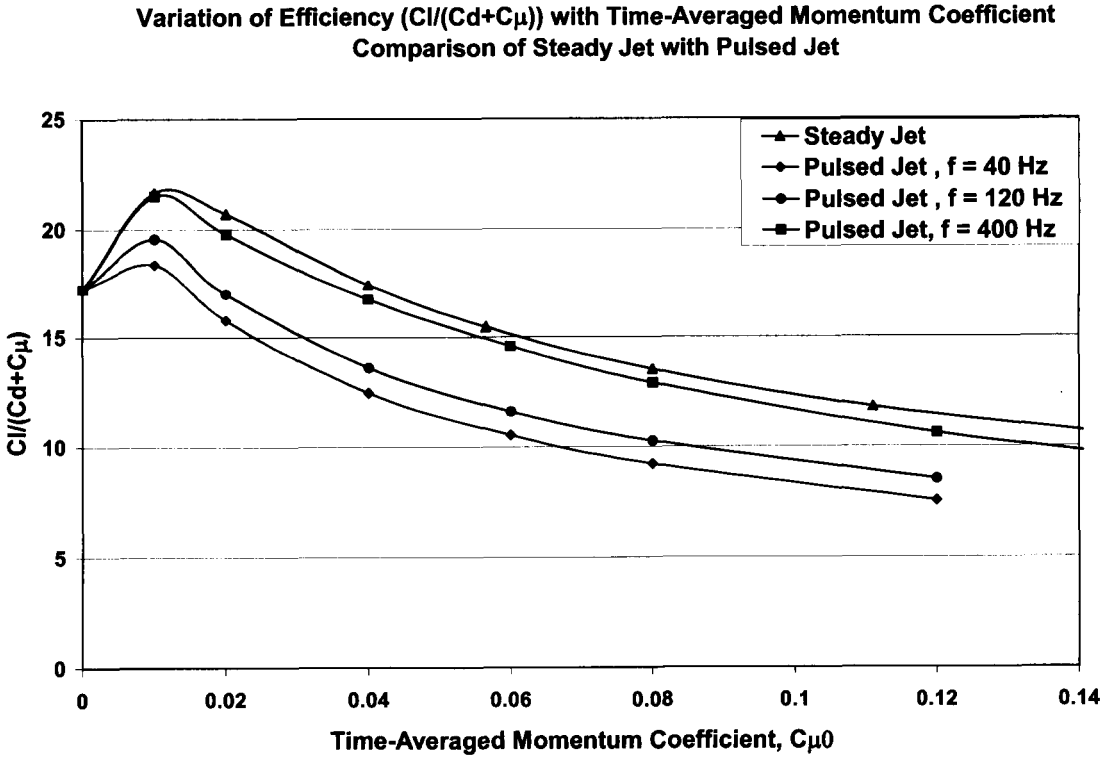

Figure 7a. Variation of Lift-to-Drag Ratio with Time-Averaged Momentum Coefficient

APPENDIX B

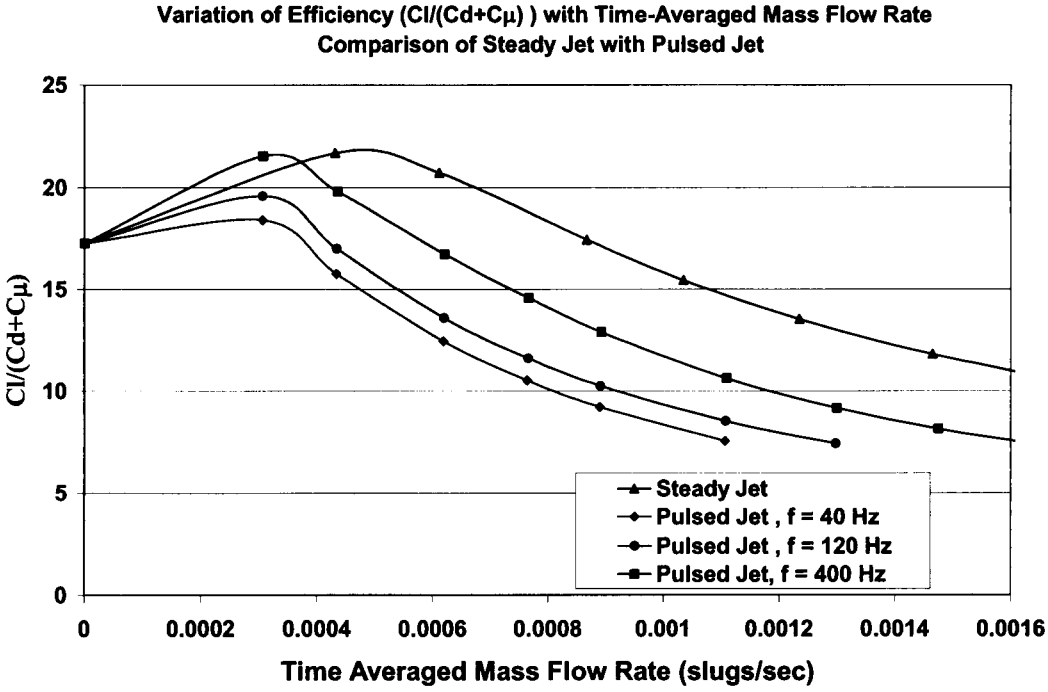

Figure 7b. Variation of Lift-to-Drag Ratio with Time-Averaged Mass Flow Rate

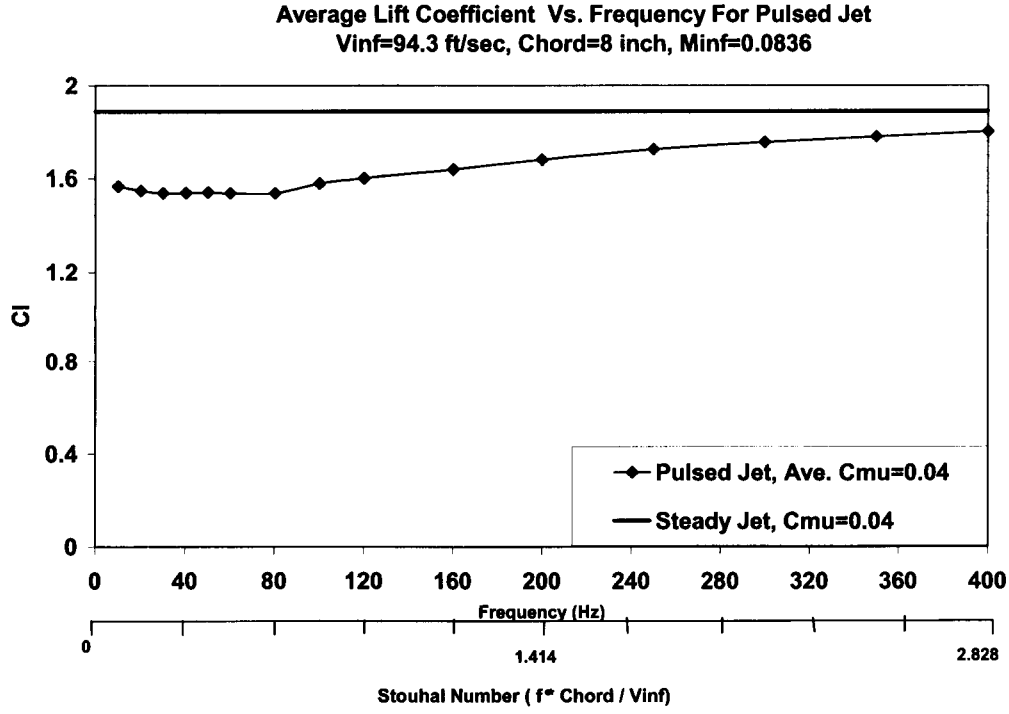

Figure 8a. Variation of C_l with Pulsed Jet Frequency at fixed Time-Averaged Momentum Coefficient

APPENDIX B

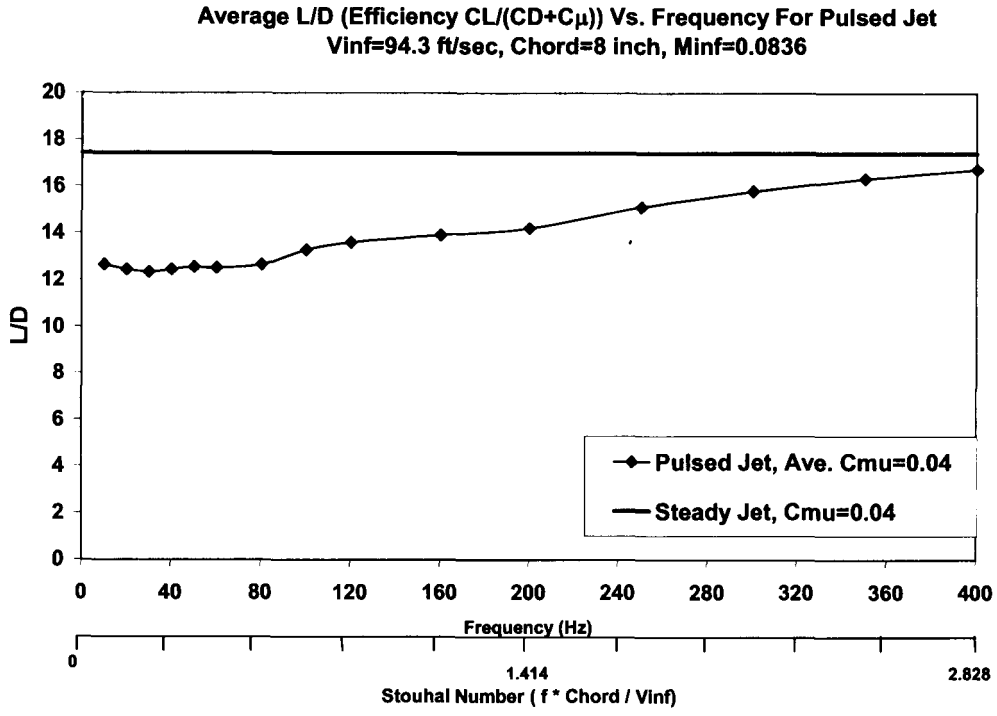

Figure 8b. Variation of L/D with Pulsed Jet Frequency at fixed Time-Averaged Momentum Coefficient